9

The Reaction Mass Pendulum (RMP) Model for Humanoid Robot Gait and Balance Control

Sung-Hee Lee
University of California, Los Angeles
Los Angeles, CA, U.S.A
sunghee@cs.ucla.edu
Ambarish Goswami
Honda Research Institute
Mountain View, CA, U.S.A
agoswami@honda-ri.com

1. Introduction

Next generation humanoids are expected to successfully coexist within human environments. This imposes very difficult challenges to the robot controller in the form of complex and flexible gait planning, truly dynamic movements, balance maintenance under unexpected environmental forces and disturbances. Manual programming of every gait and balance strategy is an extremely tedious proposition and is not practically implementable. Formulation and implementation of generic autonomous behavior, however, need a deep intuitive understanding of the fundamental humanoid dynamics.

In this regard, reduced biped models, such as the different variations of the inverted pendulum models (Kajita et al, 1992; Kajita et al, 2002; Sugihara & Nakamura, 2003; Komura et al., 2005), have been very beneficial. These models allow us to ignore the movements of the individual limbs of the humanoid, and instead, focus on two important points - the center of pressure (CoP) and the center of mass (CoM) - and the line joining them. It is customary to employ a reduced model during the planning and analysis stage and map the planned control strategy into the usual joint-level controller of the full humanoid for an implementation-ready control law. By focusing attention to the fundamental aspects of humanoid dynamics, such models open the way to new classes of control laws, which would otherwise be difficult or impossible to conceive.

A limitation of the above-mentioned reduced models is that they represent the entire humanoid body only as a point mass and do not characterize the significant centroidal moment of inertia of the humanoid body (except (Komura et al., 2005a)). The centroidal moment of inertia is a property of the distributed masses of the robot limbs (head, arms, legs, etc). We have earlier demonstrated that a humanoid's state of balance is closely related to its rotational equilibrium which, in turn, is dependent on its angular momentum rate change (Abdallah & Goswami, 2005). The centroidal moment of inertia directly contributes to the

centroidal angular momentum and its rate change. Direct manipulation of momenta is becoming a reasonable, and sometimes preferable, way to control a robot (Kajita et al., 2003; Vermeulen et al., 2006; Hofmann, 2005). The Reaction Mass Pendulum (RMP) model (Lee & Goswami, 2007), which we describe in this paper, is expected to be useful for these controllers.

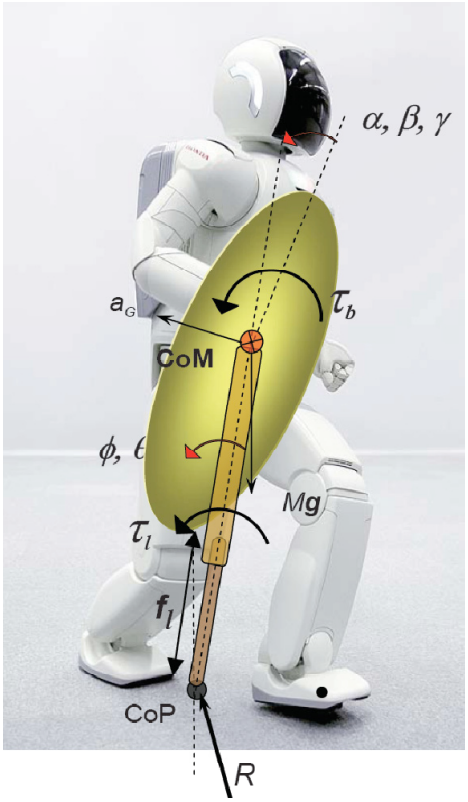

Fig. 1: Conceptual diagram of the RMP model of a humanoid. The RMP consists of a "leg" connecting the robot's CoM and CoP. The reaction mass ellipsoid, signifying the aggregate spatial inertia of the robot at its CoM, sits atop the leg. As the robot moves, the shape, size and orientation of the ellipsoid changes in a manner described in Section 2.

As shown in Fig. 1, an RMP consists of two components, a "leg" that joins the CoP and the CoM, and an ellipsoidal "body" – the abstracted reaction mass – that characterizes the inertia of the entire robot projected at the CoM. As the robot moves in space, so does the RMP, resulting in a movement of the CoP and CoM. All limb movements of the robot affect its centroidal moment of inertia, which is captured by the changing shape, size and orientation of the ellipsoidal reaction mass.

The rest of this chapter is as follows: We first provide detailed introduction and insights to the mathematical preliminaries used in this chapter (Section 2), and then derive the equations for the RMP model of a humanoid (Section 3) as well as the description of the

parameters and properties of the mechanical realization of RMP model (Section 4). Finally, we present demonstrations of the application of inertia shaping technique (Section 5) followed by conclusions and future work (Section 6).

2. Mathematical Background

In this paper, we have used a Lie Group based approach (Murray et al., 1994) to derive the details of the RMP model. In this section we introduce preliminary geometric quantities and use them to define the spatial inertia of a single rigid body. Spatial inertia is a critical quantity in our model and we later generalize this concept to a multi-body system.

2.1 Geometric Preliminaries

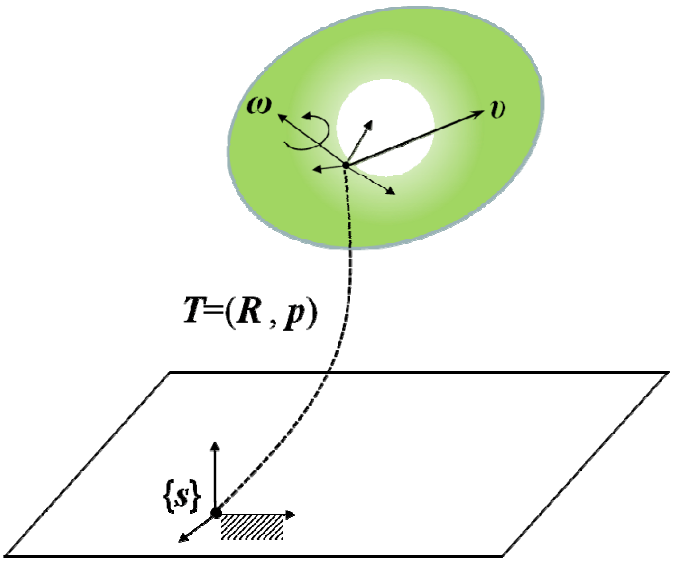

Fig. 2: A rigid body moving in space. $\boldsymbol{R}$ and $\boldsymbol{p}$ are the orientation and position of the body frame with respect to a spatial frame {s}, respectively. $\boldsymbol{\omega}$ and $\boldsymbol{v}$ are its angular and linear velocities expressed with respect to the body frame.

Let us consider a moving rigid body such as in Fig. 2. $\boldsymbol{T} = \begin{bmatrix} \boldsymbol{R} & \boldsymbol{p} \\ \boldsymbol{0} & 1 \end{bmatrix} \in SE(3)$ denotes the homogeneous transformation matrix of the body frame with respect to a spatial frame $\{s\}$, any frame fixed in space. When the body frame is moving in space, its *spatial velocity*[1] expressed with respect to the body frame (hence called *body velocity*) is defined as a twist

[1] Per (Featherstone, 1987), we use a term "spatial" to the definitions that combine angular and linear properties. For instance, a spatial velocity is the combination of the angular and linear velocities. Likewise, we will use a spatial force (the combination of torque and linear force), spatial inertia (rotational inertia and mass), and spatial momentum (angular and linear momenta). Note that in (Murray et al., 1994), the spatial velocity has different meaning; it refers to a velocity expressed with respect to a spatial frame, as opposed to the

$$\hat{\mathbf{v}} = \boldsymbol{T}^{-1}\dot{\boldsymbol{T}} = \begin{bmatrix} \boldsymbol{S}(\boldsymbol{\omega}) & \boldsymbol{v} \\ \mathbf{0} & 0 \end{bmatrix}, \tag{1}$$

which is an element of se(3), the Lie algebra of SE(3), and expressed as a 4× 4 matrix where $\boldsymbol{\omega}$ and $\boldsymbol{v}$ are its angular and linear velocities. The quantities $\boldsymbol{\omega}$ and $\boldsymbol{v}$ are expressed with respect to the instantaneous body frame. $\boldsymbol{S}(\boldsymbol{\omega})$ denotes the skew-symmetric matrix representation of $\boldsymbol{\omega} = [\omega_x, \omega_y, \omega_z]^T$; i.e.,

$$\boldsymbol{S}(\boldsymbol{\omega}) = \begin{bmatrix} 0 & -\omega_z & \omega_y \\ \omega_z & 0 & -\omega_x \\ -\omega_y & \omega_x & 0 \end{bmatrix}. \tag{2}$$

Note that, when multiplied with a vector, the skew-symmetric matrix yields the cross product, i.e., $\boldsymbol{S}(\boldsymbol{\omega})\boldsymbol{v} = \boldsymbol{\omega} \times \boldsymbol{v}$. Although represented as a 4 × 4 matrix, a twist has only 6 components; we can express a twist $\hat{\mathbf{v}}$ as a 6 dimensional vector $\mathbf{v} = [\boldsymbol{\omega}^T, \boldsymbol{v}^T]^T$ for convenience.

For all $\mathbf{s} \in$ se(3), exp ($\hat{\mathbf{s}}$) is an element of SE(3) and there exists a closed-form formula of the exponential map exp: se(3) → SE(3) (see Murray et al., 1994). When $\mathbf{s} \in$ se(3) and q ∈ ℝ refer to a screw parameter of a joint and its joint angle, exp ($\hat{\mathbf{s}}$q) represents the transformation that is made by the joint motion.[2]

Coordinate transformation of the twist is achieved by the so-called *adjoint mapping*. Given $\boldsymbol{T} \in$ SE(3) and some $\mathbf{g} = [\boldsymbol{\rho}^T, \boldsymbol{\varphi}^T]^T \in$ se(3), the adjoint mapping $\mathrm{Ad}_{\boldsymbol{T}}$: se(3) → se(3) is defined as $\mathrm{Ad}_{\boldsymbol{T}}\,\hat{\mathbf{g}} = \boldsymbol{T}\,\hat{\mathbf{g}}\,\boldsymbol{T}^{-1}$, or in matrix form as

$$\mathrm{Ad}_{\boldsymbol{T}}\,\mathbf{g} = \begin{bmatrix} \boldsymbol{R} & \mathbf{0} \\ \boldsymbol{S}(\boldsymbol{p})\boldsymbol{R} & \boldsymbol{R} \end{bmatrix} \begin{bmatrix} \boldsymbol{\rho} \\ \boldsymbol{\varphi} \end{bmatrix}. \tag{3}$$

The spatial velocity $\mathbf{v}$ with respect to {s} is given by ${}^{s}\mathbf{v} = \mathrm{Ad}_{\boldsymbol{T}}\,\mathbf{v}$.[3] Another useful operator that we use in this chapter is the Lie bracket $\mathrm{ad}_{\mathbf{v}}$: se(3) → se(3) and it occurs when $\mathrm{Ad}_{\boldsymbol{T}}$ is differentiated. The Lie bracket is defined as $\mathrm{ad}_{\hat{\mathbf{v}}_1}\hat{\mathbf{v}}_2 = \hat{\mathbf{v}}_1\hat{\mathbf{v}}_2 - \hat{\mathbf{v}}_2\hat{\mathbf{v}}_1$, or in matrix form

$$\mathrm{ad}_{\mathbf{v}_1}\mathbf{v}_2 = \begin{bmatrix} \mathbf{S}(\boldsymbol{\omega}_1) & \mathbf{0} \\ \mathbf{S}(\boldsymbol{v}_1) & \mathbf{S}(\boldsymbol{\omega}_1) \end{bmatrix} \begin{bmatrix} \boldsymbol{\omega}_2 \\ \boldsymbol{v}_2 \end{bmatrix}. \tag{4}$$

---

body velocity, which is expressed with respect to a body frame. However, we continue to use the term spatial frame to mean a ground reference frame, a frame rigidly attached to the ground.

[2] For instance, $\mathbf{s} = (\boldsymbol{a}^T, \mathbf{0}^T)^T$ for a revolute joint, where a unit vector $\boldsymbol{a} \in \mathbb{R}^3$ is the joint axis with respect to the body frame, and $\mathbf{s} = (\mathbf{0}^T, \boldsymbol{a}^T)^T$ for a prismatic joint, where $\boldsymbol{a}$ is the axis of translation.

[3] Left superscript s indicates the symbol is expressed in a spatial frame {s}. Likewise, we will use left superscript 0 and g to indicate a spatial frame that coincides with the base frame and a frame located at CoM of the humanoid robot, respectively. No left superscript is used when a symbol is expressed in the body frame.

One can easily verify that $\mathrm{Ad}_{\boldsymbol{T}}^{-1} = \mathrm{Ad}_{\boldsymbol{T}^{-1}}$ and $\mathrm{ad}_{\mathbf{v}}\mathbf{v} = \mathbf{0}$.
The spatial force $\mathbf{f} = [\boldsymbol{m}^T, \boldsymbol{f}^T]^T$ is an element of se*(3), the dual space of se(3), where $\boldsymbol{m} \in \mathbb{R}^3$ and $\boldsymbol{f} \in \mathbb{R}^3$ represent a moment and linear force, respectively. Corresponding to the adjoint mappings in se(3) space, the *dual adjoint mappings* $\mathrm{Ad}_{\boldsymbol{T}}^*: \mathrm{se}^*(3) \to \mathrm{se}^*(3)$ and $\mathrm{ad}_{\mathbf{g}}^*: \mathrm{se}^*(3) \to \mathrm{se}^*(3)$ are also defined and, in matrix form, they are the transposes of $\mathrm{Ad}_{\boldsymbol{T}}$ and $\mathrm{ad}_{\mathbf{g}}$; i.e.,

$$\begin{aligned} \mathrm{Ad}_{\boldsymbol{T}}^* &= \mathrm{Ad}_{\boldsymbol{T}}^T, \\ \mathrm{ad}_{\boldsymbol{T}}^* &= \mathrm{ad}_{\boldsymbol{T}}^T. \end{aligned} \tag{5}$$

The spatial force with respect to $\{s\}$ is given as ${}^{s}\mathbf{f} = \mathrm{Ad}_{\boldsymbol{T}^{-1}}^* \mathbf{f}$.[4]

2.2 Spatial inertia of a single rigid body

The spatial inertia of a body represents its aggregate inertial property by combining its translational mass and rotational inertia.
When a body frame is located at the CoM of a rigid body, its kinetic energy takes the following simple form,

$$E_k = \frac{1}{2} m\, \boldsymbol{v}^T \boldsymbol{v} + \frac{1}{2}\, \boldsymbol{\omega}^T \bar{\boldsymbol{I}}_{CoM} \boldsymbol{\omega}, \tag{6}$$

where m is the mass, $\bar{\boldsymbol{I}}_{CoM} \in \mathbb{R}^{3\times 3}$ is the rotational inertia matrix, and $\boldsymbol{v}$ and $\boldsymbol{\omega}$ are linear and angular velocities. We use the subscript *CoM* to stress that the reference frame is at the CoM. In terms of its spatial velocity, the kinetic energy is expressed as follows:

$$E_k = \frac{1}{2} \mathbf{v}_{CoM}^T\, \boldsymbol{I}_{CoM}\, \mathbf{v}_{CoM}, \tag{7}$$

where $\boldsymbol{I}_{CoM} = \begin{bmatrix} \bar{\boldsymbol{I}}_{CoM} & \mathbf{0} \\ \mathbf{0} & m\mathbf{1} \end{bmatrix}$ is called the spatial inertia of the rigid body. Now we consider an arbitrary body frame that is not located at the CoM. Let $\boldsymbol{G} = (\boldsymbol{R}, \boldsymbol{c}) \in \mathrm{SE}(3)$ denote a transformation matrix from this (arbitrary) body frame to a frame at the CoM where $\boldsymbol{c}$ is the position of the CoM. Since the kinetic energy is coordinate-independent,

$$E_k = \frac{1}{2} \mathbf{v}_{CoM}^T\, \boldsymbol{I}_{CoM}\, \mathbf{v}_{CoM} = \frac{1}{2} \mathbf{v}^T\, \boldsymbol{I}\, \mathbf{v}. \tag{8}$$

Substituting the relation $\mathbf{v} = \mathrm{Ad}_{\boldsymbol{T}} \mathbf{v}_{CoM}$, we can derive the structure of the spatial inertia with respect to an arbitrary body frame:

$$\begin{aligned} \boldsymbol{I} &= \mathrm{Ad}_{\boldsymbol{G}^{-1}}^*\, \boldsymbol{I}_{CoM}\, \mathrm{Ad}_{\boldsymbol{G}^{-1}} \\ &= \begin{bmatrix} \boldsymbol{R}\bar{\boldsymbol{I}}_{CoM}\boldsymbol{R}^T - m\boldsymbol{S}(\boldsymbol{c})^2 & m\boldsymbol{S}(\boldsymbol{c}) \\ -m\boldsymbol{S}(\boldsymbol{c}) & m\mathbf{1} \end{bmatrix} \\ &= \begin{bmatrix} \bar{\boldsymbol{I}} & m\boldsymbol{S}(\boldsymbol{c}) \\ -m\boldsymbol{S}(\boldsymbol{c}) & m\mathbf{1} \end{bmatrix}, \end{aligned} \tag{9}$$

[4] Note that $\mathrm{Ad}_{\boldsymbol{T}^{-1}}^* = \begin{bmatrix} \boldsymbol{R} & \boldsymbol{S}(\boldsymbol{p})\boldsymbol{R} \\ \mathbf{0} & \boldsymbol{R} \end{bmatrix}$.

where $\bar{\boldsymbol{I}} = \boldsymbol{R}\bar{\boldsymbol{I}}_{CoM}\boldsymbol{R}^T - m\boldsymbol{S}(\boldsymbol{c})^2$ is the rotational inertia matrix with respect to the body frame. Similarly, one can verify that the coordinate transformation of the spatial inertia is accomplished by pre and post multiplying the adjoint matrices. For instance, the spatial inertia with respect to the spatial frame is as follows:

$$^{s}\boldsymbol{I} = \mathrm{Ad}^{*}_{\boldsymbol{T}^{-1}}\, \boldsymbol{I}\, \mathrm{Ad}_{\boldsymbol{T}^{-1}}. \tag{10}$$

Note that $\bar{\boldsymbol{I}}$ and $\boldsymbol{I}$ are both symmetric positive definite matrices.
Having defined the spatial inertia, we can define the *spatial momentum* of the rigid body as an element of $\mathrm{se}^*(3)$ as follows:

$$\boldsymbol{h} = \begin{bmatrix}\boldsymbol{k}\\ \boldsymbol{l}\end{bmatrix} = \boldsymbol{I}\mathbf{v} \in \mathrm{se}^*(3), \tag{11}$$

where $\boldsymbol{k}$ and $\boldsymbol{l}$ are the angular and linear momenta, respectively. Substituting (9) into (11), we can derive the expressions of the angular and linear momenta; $\boldsymbol{k} = \bar{\boldsymbol{I}}\boldsymbol{\omega} + m\boldsymbol{c} \times \boldsymbol{v}$ and $\boldsymbol{l} = m(\boldsymbol{v} - \boldsymbol{c} \times \boldsymbol{\omega})$. Note that, since the spatial momentum is an element of $\mathrm{se}^*(3)$, coordinate transformation of the spatial momentum is achieved through the dual adjoint mapping. For instance, the spatial momentum with respect to $\{s\}$ is $^{s}\boldsymbol{h} = \mathrm{Ad}^{*}_{\boldsymbol{T}^{-1}}\, \boldsymbol{h}$.

3. Generating the RMP Model of a Humanoid

We generate the RMP model of a humanoid by extending the concept of spatial inertia to an articulated chain. In this section we derive the necessary equations to exploit the concept of composite rigid body (CRB) inertia and show how it relates to the momentum of a humanoid. In the next section we will outline a mechanical realization of the RMP.

3.1 CRB inertia of a humanoid robot

We assume that a humanoid robot model consists of $n + 1$ links with the base link, usually the pelvis, indexed as 0 (Fig. 3).
Let $\boldsymbol{T}_0 \in \mathrm{SE}(3)$ denote the transformation matrix of the body frame of the base link (*base frame* hereafter) and $\boldsymbol{q} = (q_1, \ldots, q_n)^T \in \mathbb{R}^n$ the joint angle vector of the robot, then $\boldsymbol{\Theta} = (\boldsymbol{T}_0, \boldsymbol{q})$ defines the position and orientation of the humanoid robot. Subsequently, $\dot{\boldsymbol{\Theta}} = (\mathbf{v}_0, \dot{\boldsymbol{q}})$ will denote the body velocity of the base frame and joint velocities.[5]
$\boldsymbol{T}_i$ denotes the transformation matrix from the spatial frame to the body frame of link i. For a non-base link, $\boldsymbol{T}_i$ $(i > 0)$ is determined by $\boldsymbol{T}_0$ and the joint angles $\boldsymbol{q}$, i.e., $\boldsymbol{T}_i = \boldsymbol{T}_0\, \boldsymbol{G}_i(\boldsymbol{q})$, where $\boldsymbol{G}_i = \boldsymbol{T}_0^{-1}\boldsymbol{T}_i$ is the transformation matrix from the base frame to link i. Note that $\boldsymbol{G}_i$ does not depend on $\boldsymbol{T}_0$ and is entirely determined by $\boldsymbol{q}$. For simplicity, we assume that, except for the base link, each link is connected to its parent link by a 1-DOF joint. Then

[5] Note that $\dot{\boldsymbol{\Theta}}$ is a slight abuse of notation because $\mathbf{v}_0$ is not $\dot{\boldsymbol{T}}_0$, but $\boldsymbol{T}_0^{-1}\dot{\boldsymbol{T}}_0$. In this representation, $\boldsymbol{\Theta}$ is not generalized coordinates because a 4×4 matrix $\boldsymbol{T}_0$ has only 6 DOFs. Another, more common way to represent the configuration of a robot is using 6 numbers (3 for the orientation and 3 for the position) instead of using a 4×4 matrix $\boldsymbol{T}_0$. An advantage of this representation is that the configuration vector is generalized coordinates as its dimension is same as the DOFs of the robot. However, since this uses 3 numbers to represent the orientation, it has singularities at certain configurations.

$\boldsymbol{T}_i = \boldsymbol{T}_{p(i)}\boldsymbol{H}_i e^{\hat{\mathbf{s}}_i q_i}$ holds for $i = 1 \ldots n$ where $p(i)$ denotes the parent link of link i, $\boldsymbol{H}_i \in \mathrm{SE}(3)$ is the transformation from $p(i)$ to i at $q_i = 0$, and $\mathbf{s}_i \in \mathrm{se}(3)$ is the screw parameter of the joint.

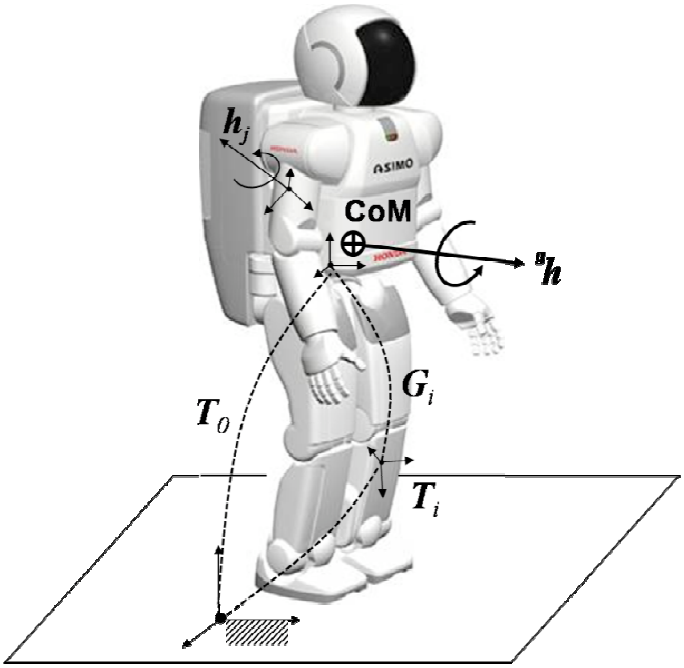

Fig. 3: T_i denotes the transformation matrix of a link i and the base link is indexed as 0. G_i is the transformation of link i as seen from the base frame and it is determined by the joint angles. The centroidal momentum of a humanoid robot $^{\boldsymbol{g}}\boldsymbol{h}$ is computed as the sum of the momenum of each link $\boldsymbol{h_i}$ expressed with respect to the CoM.

The composite rigid body (CRB) inertia (Walker & Orin, 1982) of a humanoid robot is its instantaneous spatial inertia, assuming that all of its joints are frozen. It has the same structure as the spatial inertia of a single rigid body (Eq. 9). CRB inertia is identical to the so-called locked inertia, a term that is used in geometric mechanics (Ostrowski, 1999). Mathematically, CRB inertia of a humanoid with respect to its base frame is expressed as follows:

$$\begin{aligned} {}^0\boldsymbol{I} &= \sum {}^0\boldsymbol{I}_i \\ &= \sum \mathrm{Ad}^*_{\boldsymbol{G}_i^{-1}} \boldsymbol{I}_i \, \mathrm{Ad}_{\boldsymbol{G}_i^{-1}} \end{aligned} \tag{12}$$

Next, we show how CRB inertia is related to the momentum of a humanoid robot. To this end, we first define the *link Jacobian* $\boldsymbol{J}_i$ of a link i that is similar to the manipulator Jacobian as follows;

$$\boldsymbol{J}_i = [\mathrm{Ad}_{\boldsymbol{G}_i^{-1}}\,,\ \boldsymbol{J}_{i,q}], \tag{13}$$

$$\boldsymbol{J}_{i,q} = \left[\boldsymbol{J}_{i,1}, \ldots, \boldsymbol{J}_{i,n}\right] \in \mathbb{R}^{6\times n}, \tag{14}$$

where $\hat{\boldsymbol{J}}_{i,j} = \boldsymbol{T}_i^{-1}\left(\partial \boldsymbol{T}_i / \partial q_j\right) = \boldsymbol{G}_i^{-1}\left(\partial \boldsymbol{G}_i / \partial q_j\right).$

As in Section 2.1, $\hat{\boldsymbol{J}}_{i,j}$ is the twist, a 4×4 matrix while $\boldsymbol{J}_{i,j}$ denotes its 6 dimensional vector form. Note that $\boldsymbol{J}_{i,j}$ can be computed efficiently in a recursive manner as follows;

$$\boldsymbol{J}_{i,j} = \mathrm{Ad}^{-1}_{\boldsymbol{H}_i e^{\hat{\boldsymbol{s}}_i q_i}} \boldsymbol{J}_{p(i),j} + \boldsymbol{s}_i \delta_{i,j} \quad \text{for} \quad i = 1 \ldots \mathrm{n}, \tag{15}$$

where $\delta_{i,j}$ is the Kronecker delta function and $\boldsymbol{J}_{0,j} = \boldsymbol{0}$. In (13) and (14), $\mathrm{Ad}_{G_i^{-1}}$ and $\boldsymbol{J}_{i,q}$ are the Jacobians due to the change of the base frame and joint angles respectively. Using the link Jacobian, we can decompose the velocity of $\{i\}$ into the sum of the velocity due to the base link and the one due to the joint velocities;

$$\mathbf{v}_i = \boldsymbol{J}_i \dot{\boldsymbol{\Theta}} = \mathrm{Ad}_{G_i^{-1}} \mathbf{v}_0 + \boldsymbol{J}_{i,q} \dot{\boldsymbol{q}}\,. \tag{16}$$

The spatial momentum $\boldsymbol{h}$ of the humanoid robot is the sum of spatial momentum of each link. The one with respect to the base frame [6] is

$$\begin{aligned} {}^0\boldsymbol{h} &= \sum\nolimits_i {}^0\boldsymbol{h}_i = \sum\nolimits_i {}^0\boldsymbol{I}_i\ {}^0\mathbf{v}_i \\ &= {}^0\boldsymbol{I}\mathbf{v}_0 + \textstyle\sum_i \mathrm{Ad}^{*}_{\boldsymbol{G}_i^{-1}} \boldsymbol{I}_i \boldsymbol{J}_{i,q} \dot{\boldsymbol{q}} \\ &= {}^0\boldsymbol{I}\,(\,\mathbf{v}_0 + \mathbf{A}\dot{\boldsymbol{q}}\,) \end{aligned} \tag{17}$$

where $\mathbf{A}(\boldsymbol{q})$ is the so-called *mechanical connection* (Ostrowski, 1999). As can be seen in (17), the CRB inertia contributes directly to the spatial momentum of a robot via the mechanical connection.

While the CRB inertia can be expressed with respect to any frame, it is particularly interesting to express it at the CoM since it is related to the centroidal angular momentum (Fig. 3). The CRB inertia expressed at the humanoid CoM is called the *centroidal* CRB inertia. To denote this we use ${}^g\boldsymbol{I}$ in the RMP model.

3.2 Equimomental ellipsoids

The association of the rigid body inertia to an ellipsoid is well known and has been thoroughly exploited in physics and engineering (Crandall et al., 1982). As a straightforward extension we determine the ellipsoid associated with the centroidal CRB inertia of an articulated chain. Instead of using the kinetic energy ellipsoid, which is traditionally described with an inertia, we derive the *equimomental* ellipsoid corresponding to a CRB inertia.

Two inertias are said to be equimomental if their moments of inertia about any arbitrary axis are equal (Beer & Johnson, 1984). The equimomental ellipsoid of a rigid body is an

[6] More precisely, a spatial frame that instantaneously coincides with the base frame.

ellipsoid with a uniform density set as the mean density of the body and having the same rotational inertia about any arbitrary axis as that of the rigid body. Kinetic energy ellipsoid characterizes the torque needed to rotate the body *about* an axis whereas the equimomental ellipsoid reflects the mass distribution *along* an axis.

We prefer the uncommon equimomental ellipsoid over the well-known kinetic energy ellipsoid because the shape of the former approximates the mass distribution of the overall multi-body system. For example, the ellipsoid for an upright humanoid will be long and narrow, thereby rendering some gross geometric resemblance to the humanoid. This is not the case for the kinetic energy ellipsoid.

Let $(\sigma_1, \sigma_2, \sigma_3)$ denote the eigenvalues of the rotational inertia, and (a_1, a_2, a_3) denote the semi-axes of the equimomental ellipsoid. From the relationships $\sigma_i = m(a_j^2 + a_k^2)/5$ and $m = 4\pi a_1 a_2 a_3 \rho/3$, where ρ is the mean density, we can derive the following:

$$a_i = \left(\frac{15}{8\pi\rho}\right)^{1/5} \frac{(-\sigma_i+\sigma_j+\sigma_k)^{2/5}}{\{(\sigma_i-\sigma_j+\sigma_k)(\sigma_i+\sigma_j-\sigma_k)\}^{1/10}} \tag{18}$$

for $i, j, k = 1 \ldots 3$ and $i \neq j \neq k$.

3.3 Simulation results

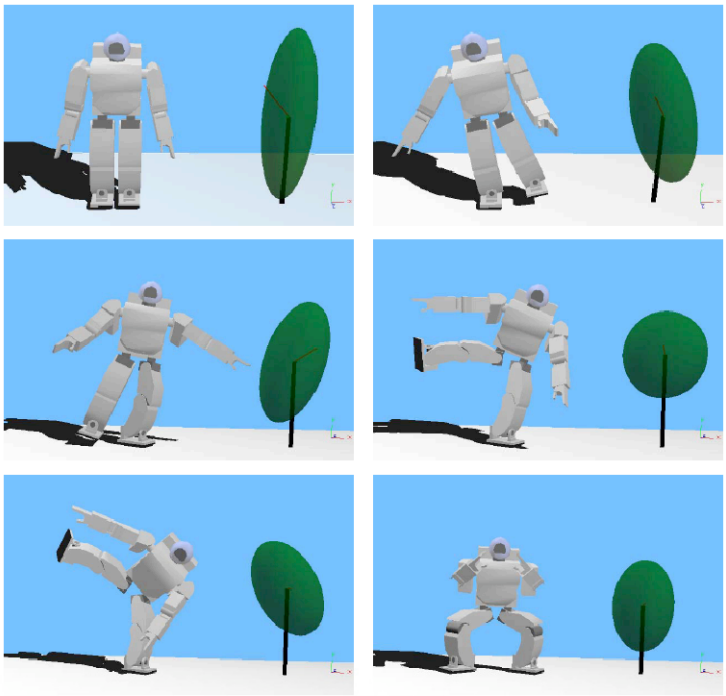

Fig. 4: Snapshots of HOAP2 robot performing Sumo-style motion superposed with corresponding RMP models. The reaction mass geometry undergoes significant changes during this motion.

The process of mapping a humanoid to its corresponding RMP involves the computation of 1) CoM, 2) CoP, and 3) centroidal CRB inertia, using robot kinematic and dynamic parameters, as well as motion data.[7] Refer to the Appendix for the computation of the CoP. We simulated the Fujitsu HOAP2 biped model, for which the parameters for some dramatic movements are available (Cominoli, 2005). The simulation is implemented using Webots (www.cyberbotics.com), a commercial simulation software.
Fig. 4 shows snapshots of HOAP2 executing Sumo-style movements. Notice the significant changes in the shape, size and orientation of the reaction mass ellipsoid[8] as the robot moves through different phases of its motion. Since the robot→RMP is a mapping to a lower dimension, different poses of the robot, at least theoretically, may get mapped to the same RMP.

4. Properties and Parameters of RMP

We have now shown how a humanoid robot can be reduced to an RMP. In this section we will discuss the realization of a mechanical model of the RMP. The RMP is the generalized 3D version of the 2D *reaction wheel pendulum* which has been studied before (Astrom et al., 2001; Olfati-Saber, 2001; Spong et al., 2001). A reaction wheel pendulum can be constructed by attaching an actuated reaction wheel to a rigid rod. The inclination angle of the pendulum can be controlled by controlling the angular acceleration of the reaction wheel. The reaction wheel, which is also called an inertia wheel, is one of a number of standard momentum exchange devices that are used to control satellite orientation (Sidi, 1997).

4.1 Description of RMP

The present work can be identified with those of [18, 19], where the benefit of a reaction mass feature of the humanoid as a mean to stabilize lateral biped dynamics is indicated. The current work is closest in spirit to the recently introduced inverted pendulum model with angular momentum properties (AMPM) (Komura et al., 2005 (a; b)). We seek to propose a physical model characterizing angular momentum.
The RMP *mathematical* model discussed here is not to be confused with the actual placement of a *physical* reaction mass device for the control of humanoid balance, as was done in (Mayer et al., 2005).
The 3D reaction mass may have continuously variable spatial inertia. At any given configuration of the robot, the centroidal CRB inertia can be reduced to an ellipsoid. This is modeled, as shown in Fig. 5 by three pairs of point masses linearly actuated along the three principal orthogonal directions of the ellipsoid. Along each axis k, the distance between the point masses is $2r_k$. The masses of each pair are always equi-distant from the ellipsoid center. The CoM of the ellipsoid is therefore always fixed at its center. The six point masses can have equal mass, i.e., $m = M/6$, so that they sum up to total mass of the humanoid robot. The distance between the masses depends on its corresponding rotational inertia, as each axis generates a moment of inertia mr_k^2.

[7] Refer to Appendix for equations to compute CoP.
[8] Reaction mass ellipsoid is synonymous with the equimomental inertia ellipsoid derived from the centroidal CRB inertia matrix.

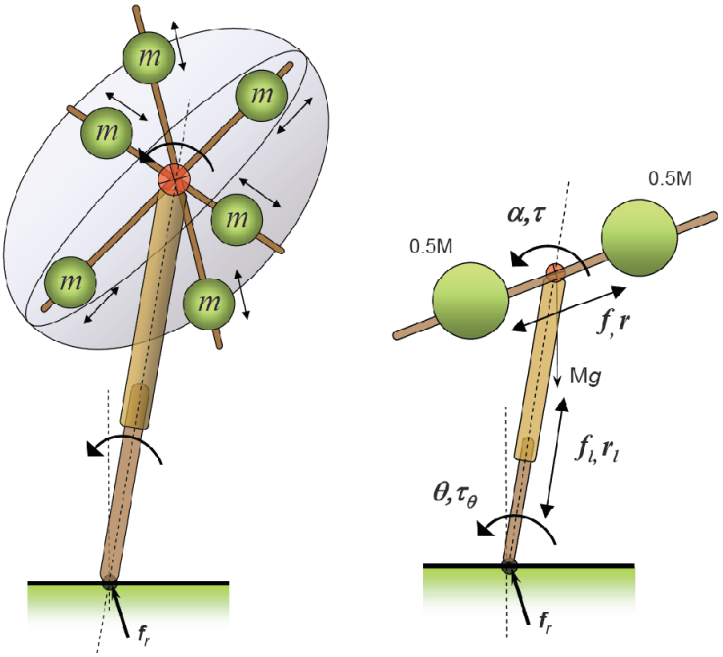

Fig. 5: (left) Conceptual mechanical realization of the 3D RMP. The gyrating ellipsoid is dynamically equivalent to three pairs of equal point masses at different radial distances that are actuated to slide on their linear tracks. The overall frame consisting of the three pairs of mutually perpendicular linear tracks form the skeleton which can be rotationally actuated in three DOFs. (right) 2D Reaction Wheel Pendulum Model. The distance between the two point masses is $\mathbf{2}\boldsymbol{r}$.

Physical description	Generalized coordinates (forces)	
	2D	3D
Radial distances of three pairs of point masses forming the ellipsoid and their actuation on linear tracks	$r\ (f)$	$r_1, r_2, r_3\ (f_1, f_2, f_3)$
Orientation angles of the ellipsoid body and their actuation	$\alpha\ (\tau)$	$\alpha, \beta, \gamma\quad (\tau_1, \tau_2, \tau_3)$
Leg length and its actuation	$r_l\ (f_l)$	$r_l\ (f_l)$
Leg orientation angles and their actuation	$\theta\ (\tau_\theta)$	$\theta, \phi\ (\tau_\theta, \tau_\phi)$
CoP position and ground reaction force	$x_{CoP}\ (R_x, R_y)$	x_{CoP}, y_{CoP} (R_x, R_y, R_z)

Table 1: Generalized variables of RMP. 2D reaction wheel pendulum model has 5 DOFs whereas 3D RMP has 11 DOFs.

The radial movement of the point masses only affects the shape and size of the ellipsoid. When $r_k = 0$ for $k = 1,2,3$ the ellipsoid reduces to a point mass and the RMP reduces to a 3D inverted pendulum. The list of all eleven generalized coordinates and nine generalized forces are listed in Table. 1.

4.2 2D Reaction wheel pendulum model

The 2D version of the RMP is equivalent to a reaction wheel pendulum, for which a realization is shown in Fig. 5(right). The generalized coordinates and generalized forces for this model are (θ, α, r_l, r) and $(\tau_\theta, \tau, f_l, f)$, respectively. The total mass of the pendulum is $0.5M + 0.5M = M$, whereas its rotational inertia about CoM is $\bar{I} = Mr^2$. The kinetic energy E_k and the potential energy E_p of the system are as follows,

$$E_k = \frac{1}{2}M\left(\dot{r}_l^2 + \dot{r}^2\right) + \frac{1}{2}Mr_l^2\dot{\theta}^2 + \frac{1}{2}Mr^2(\dot{\theta}^2 + \dot{\alpha}^2), \tag{19}$$

$$E_p = Mgr_l\sin\theta.$$

From the above relations, the equations of motion of this model are derived using Lagrangian techniques.

$$f_l = M\ddot{r}_l - Mr_l\dot{\theta}^2 + Mg\sin\theta \tag{20}$$

$$f = M\ddot{r} - Mr(\dot{\theta} + \dot{\alpha})^2 \tag{21}$$

$$\tau_\theta = Mr_l^2\ddot{\theta} + Mr^2(\ddot{\theta} + \ddot{\alpha}) + 2Mr_l\dot{r}_l\dot{\theta} + 2Mr\dot{r}(\dot{\theta} + \dot{\alpha}) + Mgr_l\cos\theta \tag{22}$$

$$\tau = Mr^2(\ddot{\theta} + \ddot{\alpha}) + 2Mr\dot{r}(\dot{\theta} + \dot{\alpha}). \tag{23}$$

The ground reaction force to the reaction mass pendulum is $\boldsymbol{f}_{\mathrm{r}} = M(\ddot{\boldsymbol{r}}_l - \mathbf{g})$. We can also relate the rate of change of the angular momentum in terms of the generalized coordinates; i.e., $\tau = \dot{k}_G$ and $\tau_\theta = \dot{k}_P + Mgr_l\cos\theta$, where the angular momentum at CoM, $k_G = \bar{I}(\dot{\theta} + \dot{\alpha})$ and the one at CoP, $k_P = k_G + Mr_l^2\dot{\theta}$.

As known, a reaction wheel pendulum can have interesting dynamics. For example, if we set $\tau_\theta = 0$, $\dot{\theta} = \ddot{\theta} = 0$, then we can compute τ that keeps $\theta = \theta_c$ stationary, i.e., $\tau = -Mgr\cos\theta_c$. The torque creates an angular acceleration $\ddot{\alpha}$ which cannot continue indefinitely due to robot joint limits. However, the example showcases the situation where the robot "leg" can be in static stability while the CoM ground projection is outside of the support base.

5. Inertia Shaping: an RMP-Based Controller

A humanoid robot has a large number of DOFs: for example, the Fujitsu HOAP2 robot has 25 DOFs and the Honda humanoid Asimo has 27 DOFs. In order to kinematically transform an RMP back to a humanoid robot, one needs to generate a map from the 11 dimensional RMP space to the much larger robot kinematics space. A unique mapping will need additional constraints, such as in the form of desired hand or foot position.

In this section, we introduce the inertia shaping technique, an iterative method to compute joint angles to create the desired CRB inertia. To this end, we first derive the relationship

between the joint angles and the CRB inertia of a humanoid robot. We call this the CRB inertia Jacobian. Specifically, since the number of independent joint angles of a humanoid robot differs according to its ground contact configuration due to the geometric constraints induced by the ground-robot contact, we formulate the CRB inertia Jacobian per each ground contact case.

5.1 CRB inertia Jacobian

Since the CRB inertia has the form of a matrix, its Jacobian should be a multi-dimensional tensor. Therefore, we string out the nonzero elements of a matrix of the CRB inertia so as to simplify the form of its Jacobian. The "strung out" vector corresponding to the spatial inertia matrix is $\check{\boldsymbol{I}} = (\check{\bar{\boldsymbol{I}}}^T, m\boldsymbol{r}^T)^T \in \mathbb{R}^9$ and $\check{\bar{\boldsymbol{I}}} = (I_{xx}, I_{xy}, I_{xz}, I_{yy}, I_{yz}, I_{zz})^T$. The first six elements correspond to rotational inertia and the last three elements to CoM multiplied by its mass.

In order to express the relation between a small change in CRB inertia and that of the generalized coordinates, we define the *CRB inertia Jacobian* $\boldsymbol{J_I}$ such that

$$\delta^s \check{\boldsymbol{I}} = \boldsymbol{J_I} \delta \boldsymbol{\Theta}. \tag{24}$$

Later on, the CRB inertia Jacobian will be used for solving the inverse problem, i.e., finding generalized coordinates corresponding to the given CRB inertia. In the following sections, we use $\boldsymbol{I}$ in the spatial frame without using superscripts. The CRB inertia Jacobian is decomposed into two parts, $\boldsymbol{J_I} = [\, \boldsymbol{J_{I,0}} \;\; \boldsymbol{J_{I,q}}]$, where $\boldsymbol{J_{I,0}} \in \mathbb{R}^{9\times 6}$ and $\boldsymbol{J_{I,q}} \in \mathbb{R}^{9\times n}$ map the motion of the base frame and the joint angles, respectively, to the rate of change of the CRB inertia; i.e.,

$$\delta \check{\boldsymbol{I}} = \boldsymbol{J_{I,0}}(\boldsymbol{T}_0^{-1}\delta \boldsymbol{T}_0) + \boldsymbol{J_{I,q}} \delta \boldsymbol{q}\,. \tag{25}$$

Specifically,

$$\boldsymbol{J_{I,0}} = \left(\boldsymbol{J_{T_0,1}}, \cdots, \boldsymbol{J_{T_0,6}}\right), \text{where } \boldsymbol{J_{T_0,i}} = \dot{\boldsymbol{I}}\,|_{\mathbf{v}=e_i,\dot{\boldsymbol{q}}=\mathbf{0}}$$

$$\boldsymbol{J_{I,q}} = \left(\boldsymbol{J_{q_1}}, \cdots, \boldsymbol{J_{q_n}}\right), \text{where } \boldsymbol{J_{q_i}} = \partial \check{\boldsymbol{I}} / \partial q_i.$$

Using the relations $\partial \mathrm{Ad}_{\boldsymbol{G}_i} / \partial q_j = \mathrm{Ad}_{\boldsymbol{G}_i} \mathrm{ad}_{\boldsymbol{J}_{i,j}} = \mathrm{ad}\,{}_{\boldsymbol{J}_{i,j}} \mathrm{Ad}_{\boldsymbol{G}_i}$ where $\hat{\boldsymbol{J}}_{i,j} = \boldsymbol{G}_i^{-1}\, \partial \boldsymbol{G}_i / \partial q_j$ [9] as defined in (14), we can derive analytical expression for $\dot{\boldsymbol{I}}$ and $\partial I / \partial q_j$; i.e.,

$$\dot{\boldsymbol{I}}|_{\dot{q}=0} = -\mathrm{ad}^*{}_{\mathbf{v}_0}\, {}^0\boldsymbol{I} - {}^0\boldsymbol{I}\, \mathrm{ad}\,{}_{\mathbf{v}_0} \tag{26}$$

$$\partial \boldsymbol{I} / \partial q_j = -\sum_{i=1}^{n} \left(\mathrm{ad}^*{}_{\boldsymbol{J}_{i,j}}\, \boldsymbol{I}_i + \boldsymbol{I}_i \mathrm{ad}\,{}_{\boldsymbol{J}_{i,j}}\right). \tag{27}$$

---

[9] One can easily prove the relations by using $\hat{\boldsymbol{J}}_{i,j} = \begin{bmatrix} \boldsymbol{R}_i^T \frac{\partial \boldsymbol{R}_i}{\partial q_j} & \boldsymbol{R}_i^T \frac{\partial \boldsymbol{p}_i}{\partial q_j} \\ \mathbf{0} & 0 \end{bmatrix}$ where $\boldsymbol{G}_i = (\boldsymbol{R}_i, \boldsymbol{p}_i)$. Also, note that $\frac{d}{dt}\mathrm{Ad}_{\boldsymbol{T}} = \mathrm{Ad}_{\boldsymbol{T}} \mathrm{ad}_{\mathbf{v}} = \mathrm{ad}\,{}_{\mathbf{v}} \mathrm{Ad}_{\boldsymbol{T}}$ where $\hat{\mathbf{v}} = \boldsymbol{T}^{-1}\dot{\boldsymbol{T}}$.

Note that the CRB inertia Jacobian includes the CoM Jacobian, i.e., the mapping from the rate of change of generalized coordinates to that of the CoM position. If we partition $\boldsymbol{J_I}$ into $\boldsymbol{J_I} = [\boldsymbol{J_I^T}\ \boldsymbol{J_G^T}]^T$ where $\boldsymbol{J_G}$ consists of the bottom 3 rows of $\boldsymbol{J_I}$, we get

$$m\dot{\boldsymbol{r}}_{\boldsymbol{G}} = \boldsymbol{J_G}\dot{\boldsymbol{\Theta}}. \tag{28}$$

$\boldsymbol{J_G}$ maps the generalized velocity to the linear momentum of the system. In fact, it is the same as the CoM Jacobian scaled by the total mass.

5.2 CRB inertia Jacobian of humanoid

If the humanoid robot is not in contact with any external environment, (25) completely describes the CRB inertia Jacobian. Otherwise, however, geometric constraints arise among the generalized coordinates, and it is advantageous to describe the CRB inertia Jacobian in terms of independent coordinates.

Let us assume $\boldsymbol{q}$ comprises $\boldsymbol{q} = (\boldsymbol{q}_r^T\ \boldsymbol{q}_l^T\ \boldsymbol{q}_t^T)^T$, where $\boldsymbol{q}_{\{r,l\}} \in \mathbb{R}^6$ are joint angle vectors for right and left legs, respectively, and $\boldsymbol{q}_t$ is for the rest of joints. We also decompose $\boldsymbol{J_I}$ accordingly; i.e.,

$$\boldsymbol{J_I} = \begin{bmatrix} \boldsymbol{J}_{\bar{\boldsymbol{I}}_0} & \boldsymbol{J}_{\bar{\boldsymbol{I}}_r} & \boldsymbol{J}_{\bar{\boldsymbol{I}}_l} & \boldsymbol{J}_{\bar{\boldsymbol{I}}_t} \\ \boldsymbol{J}_{\boldsymbol{G}_0} & \boldsymbol{J}_{\boldsymbol{G}_r} & \boldsymbol{J}_{\boldsymbol{G}_l} & \boldsymbol{J}_{\boldsymbol{G}_t} \end{bmatrix}. \tag{29}$$

We describe CRB inertia Jacobian for each ground contact case.

5.2.1 Free floating

When a humanoid robot is floating in the air, all components of the generalized coordinates are independent. Rewriting (25), we get

$$\delta\breve{\boldsymbol{I}} = \boldsymbol{J}_{\bar{\boldsymbol{I}}_0}(\boldsymbol{T}_0^{-1}\delta\boldsymbol{T}_0) + [\boldsymbol{J}_{\bar{\boldsymbol{I}}_r}\ \boldsymbol{J}_{\bar{\boldsymbol{I}}_l}\ \boldsymbol{J}_{\bar{\boldsymbol{I}}_t}]\delta\boldsymbol{q} \tag{30}$$

$$m\delta\boldsymbol{r}_{\boldsymbol{G}} = \boldsymbol{J}_{\boldsymbol{G}_0}(\boldsymbol{T}_0^{-1}\delta\boldsymbol{T}_0) + [\boldsymbol{J}_{\boldsymbol{G}_r}\ \boldsymbol{J}_{\boldsymbol{G}_l}\ \boldsymbol{J}_{\boldsymbol{G}_t}]\delta\boldsymbol{q} \tag{31}$$

Note that since we compute the CRB inertia with respect to a spatial frame, the configuration of the base frame affects the CRB inertia Jacobian. If we were only interested in the local "shape" of inertia, we need to transform the reference frame to the base frame, in which case the CRB inertia Jacobian is wholly determined by joint angles.

5.2.2 Single support by left or right foot

Let us suppose the humanoid robot is supported by one foot link, left foot link for example, which is stationary with respect to the ground. Then we can describe the constraint as follows,

$$\boldsymbol{T}_l^{-1}\delta\boldsymbol{T}_l = 0 \tag{32}$$

where $\boldsymbol{T}_l$ is the transformation matrix for the left foot link. Eq. 32 constrains that the left foot link should not move. From $\boldsymbol{T}_l = \boldsymbol{T}_0\,\boldsymbol{G}_l(\boldsymbol{q})$, where $\boldsymbol{G}_l(\boldsymbol{q})$ expresses the forward kinematic relation between the base frame and the left foot link, we can derive the following relation by plugging the relation into (32),

$$\boldsymbol{T}_0^{-1}\delta\boldsymbol{T}_0 = -\mathrm{Ad}_{\boldsymbol{G}_l}\boldsymbol{J}_l\delta\boldsymbol{q}\,. \tag{33}$$

Defining $\boldsymbol{J}_l^*$ such that $\mathrm{Ad}_{\boldsymbol{G}_l}\boldsymbol{J}_l\delta\boldsymbol{q} = \boldsymbol{J}_l^*\delta\boldsymbol{q}_l$, the CRB inertia Jacobian is written with respect to the joint angles,

$$\delta\check{\bar{\boldsymbol{I}}} = \begin{bmatrix}\boldsymbol{J}_{\bar{I}_r} & \left(\boldsymbol{J}_{\bar{I}_l} - \boldsymbol{J}_{\bar{I}_0}\boldsymbol{J}_l^*\right) & \boldsymbol{J}_{\bar{I}_t}\end{bmatrix}\delta\boldsymbol{q}, \tag{34}$$

$$m\delta\boldsymbol{r}_{\boldsymbol{G}} = \begin{bmatrix}\boldsymbol{J}_{\boldsymbol{G}_r} & \left(\boldsymbol{J}_{\boldsymbol{G}_l} - \boldsymbol{J}_{\boldsymbol{G}_0}\boldsymbol{J}_l^*\right) & \boldsymbol{J}_{\boldsymbol{G}_t}\end{bmatrix}\delta\boldsymbol{q}\,. \tag{35}$$

5.2.3 Double support

When both feet are stationary to the ground, we have an additional constraint $\boldsymbol{J}_l^*\delta\boldsymbol{q}_l = \boldsymbol{J}_r^*\delta\boldsymbol{q}_r$, where $\boldsymbol{J}_r^*$ of the right foot link corresponds to $\boldsymbol{J}_l^*$ of the left foot. This constraint yields $\delta\boldsymbol{q}_r = \boldsymbol{J}_r^{*-1}\boldsymbol{J}_l^*\delta\boldsymbol{q}_l$. Therefore,

$$\delta\check{\bar{\boldsymbol{I}}} = \begin{bmatrix}\left\{\boldsymbol{J}_{\bar{I}_l} + \left(\boldsymbol{J}_{\bar{I}_r}\boldsymbol{J}_r^{*-1} - \boldsymbol{J}_{\bar{I}_0}\right)\boldsymbol{J}_l^*\right\} & \boldsymbol{J}_{\bar{I}_t}\end{bmatrix}\begin{bmatrix}\delta\boldsymbol{q}_l \\ \delta\boldsymbol{q}_t\end{bmatrix} \tag{36}$$

$$m\delta\boldsymbol{r}_{\boldsymbol{G}} = \begin{bmatrix}\left\{\boldsymbol{J}_{\boldsymbol{G}_l} + \left(\boldsymbol{J}_{\boldsymbol{G}_r}\boldsymbol{J}_r^{*-1} - \boldsymbol{J}_{\boldsymbol{G}_0}\right)\boldsymbol{J}_l^*\right\} & \boldsymbol{J}_{\boldsymbol{G}_t}\end{bmatrix}\begin{bmatrix}\delta\boldsymbol{q}_l \\ \delta\boldsymbol{q}_t\end{bmatrix}. \tag{37}$$

5.3 Inertia shaping

An interesting application of our RMP modeling approach is what we call *inertia shaping* of an articulated chain (Lee & Goswami, 2007). Inertia shaping is a high-level approach to precisely control the aggregate kino-dynamic characteristics of an articulated chain by controlling its CRB inertia. Given a desired CRB inertia $\boldsymbol{I}_d$ of the robot, the inertia shaping controller seeks to determine the proper configuration of the robot that attains it. This can be posed as an inverse kinematics problem with the desired CRB inertia constraints. Since we have derived the CRB inertia Jacobian, the inverse kinematics problem can be solved by any suitable optimization algorithm. One solution will be to iteratively update the desired joint angles using pseudo-inverse of the centroidal CRB inertia Jacobian (24), i.e.,

$$\delta\boldsymbol{\Theta}_I = \boldsymbol{J}_I^{\dagger}\delta(\check{\boldsymbol{I}}_d - \check{\boldsymbol{I}}\,), \tag{38}$$

where $\boldsymbol{\Theta}_I$ is the vector of independent generalized coordinates and $\boldsymbol{J}_I^{\dagger} = \boldsymbol{J}_I^T(\boldsymbol{J}_I\boldsymbol{J}_I^T)^{-1}$. This is the simplest form of inertia shaping that does not consider additional constraints such as obstacles in the environment or self-collision.

For the inertia shaping algorithm to be applied to actual humanoid robots, more sophisticated algorithm can be developed. For example, we may need to incorporate inverse kinematics problems into the inertia shaping process. The CRB inertia Jacobian provides useful information on the rate of change of the CRB inertia as a function of generalized coordinates, which is necessary in any iterative gradient-based algorithms for computing optimal joint angles to achieve desired inertia.

Fig. 6 presents three examples of inertia shaping on a non-contacting Asimo-like floating in space (say, a humanoid astronaut). The robot is given three different commands, shown in series a, b, and c, respectively, to try to match its own CRB inertia to a desired CRB inertia. Starting from an initial configuration, the robot moves its joints such that the cost function,

considered to be the Frobenius norm of the difference between the two inertia matrices, is minimized. Specifically, we deal with the inertia with respect to the base frame, hence controlling joint angles is sufficient.

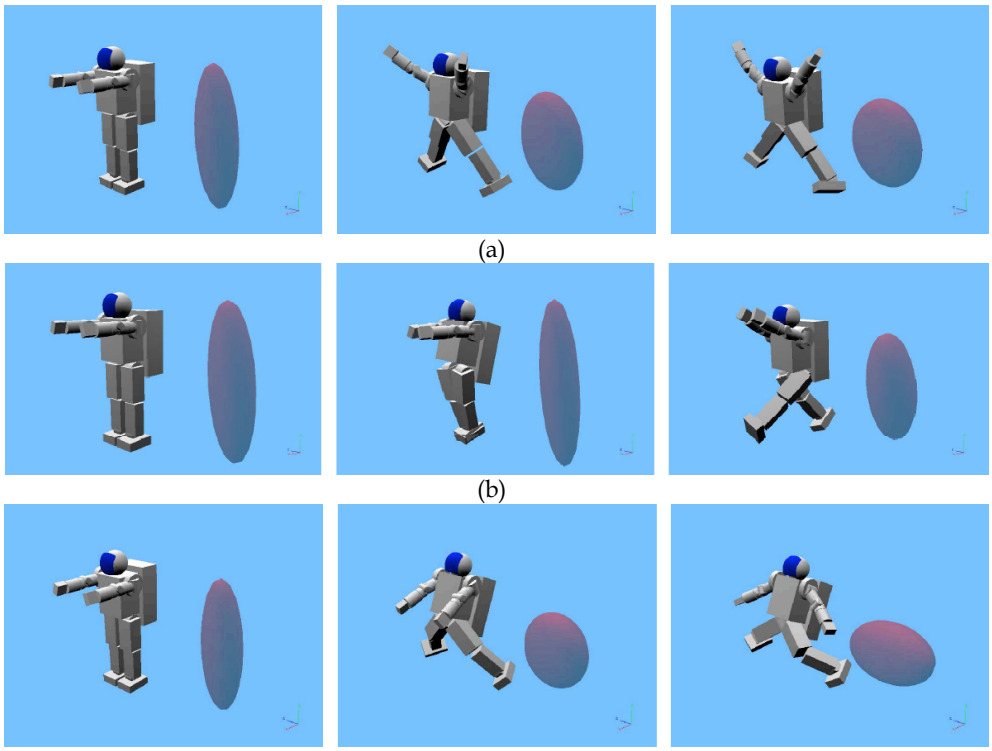

Fig. 6: Demonstration of the inertia shaping technique on a non-contacting biped robot floating in space. A floating robot has no CoP, so the RMP reduces to simply the ellipsoidal reaction mass.

In Fig. 6 (a) the desired inertia components along all three axes are equal and large. Hence the robot tries to "expand" in all directions. In Fig. 6 (b) the desired inertia in Y-component (vertical) is big, and the other components are very small. In Fig. 6 (c) robot tries to make its inertia in X and Z-components large.

This simulation demonstrates the important point of effectively controlling a complex biped with a very simple control law. While the robot model has 27 dofs, the control law deals with only three variables which are the three diagonal elements of the robot's rotational inertia.

In Fig. 7, we specify only desired CoM (Eq. 37) while keeping desired rotational inertia (Eq. 36) unconstrained. The inertia shaping algorithm computes optimal joint angles that creates specified CoM. In this example, we kept the joint angles for the arm and head fixed and moved only leg joints. Since we keep the ground projection of CoM within the support

polygon, the humanoid robot maintains balance even in relatively extreme pose (e.g., bottom right figure).

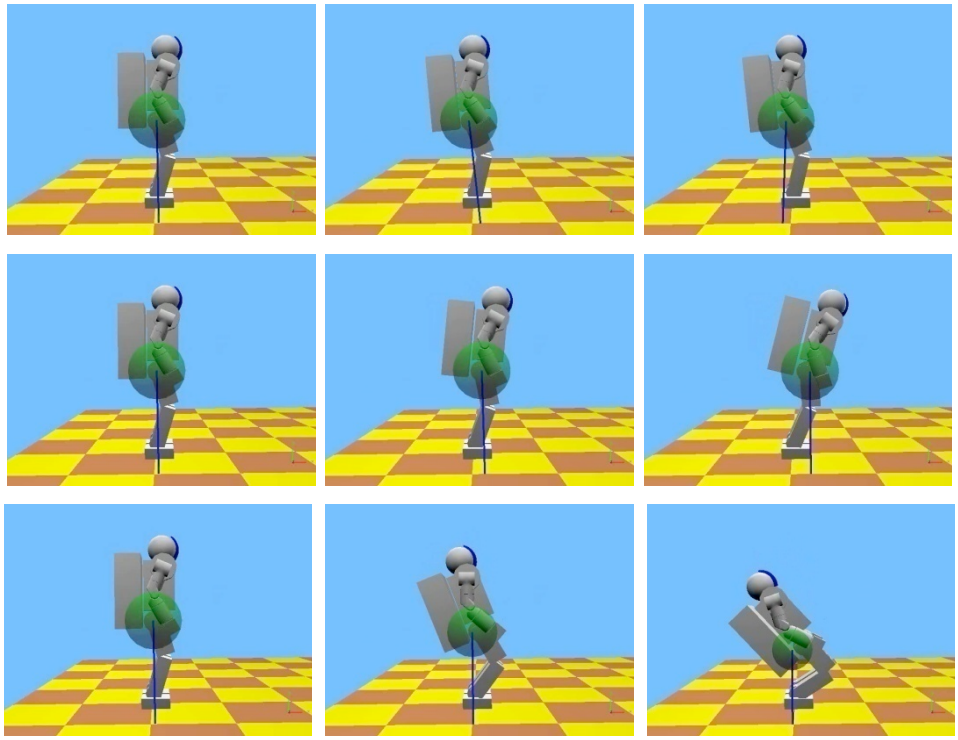

Fig. 7: Given desired CoM position, the inertia shaping algorithm computes optimal joint angles to achieve the goal. In this demonstration, desired CoM is specified such that it moves gradually backward (top), forward (middle), and downward (bottom). Blue line segments connect CoP to CoM and radius of the green circle represents rotational inertia at CoM about Z-axis which is pointed towards the reader.

6. Conclusions and Future Work

We have introduced the reaction mass pendulum (RMP) model of a humanoid robot. The RMP model contains an actuated ellipsoidal reaction mass to explicitly model the robot's angular momentum. The ellipsoid represents the composite rigid body (CRB) inertia of the robot computed at its CoM. The reaction mass is an addition to the existing inverted pendulum humanoid models that only consider a point mass, and is also a mechanical realization of the AMPM model that accounts for the presence of centroidal angular momentum. The RMP is an instantaneous 3D capture of the aggregate kinematics and dynamics of a general humanoid robot. As a lower-dimensional (n = 11) dynamic equivalent of a high dof humanoid it lends itself to more probing analysis for dynamics and planning.

We presented the technique of inertia shaping, which can be thought of as a kino-dynamics-based higher-level control for humanoid. We have provided detailed formulations for each ground contact configuration and demonstrated the successful application to a free floating case as well as the CoM control in double support case.
RMP is introduced mainly as an analysis tool. For it to be a worthwhile successor to the very useful linear inverted pendulum (LIPM) or AMPM models, one need to develop an algorithm to compute desired trajectory of RMP. Our mechanical realization of the RMP model can be useful for developing such control laws. Also, we feel that analyzing RMP motion of human walking motion may provide a useful insight for this.
Once the planning is performed, one need to formulate control laws to apply desired RMP motion to humanoids. Inertia shaping can be used for this process, but more factors such as joint limits, collision with external objects, and prioritization of joints would have to be considered for a humanoid robot to perform various tasks while interacting with the environments (e.g., walking while holding a cup with the hand). This work is ongoing.

7. Acknowledgement

We appreciate Kangkang Yin for correcting errors in the original paper (Lee & Goswami, 2007). Ambarish appreciates fruitful discussions with Jerry Pratt, David Orin and especially with Stefano Stramigioli.

8. Appendix

8.1 Computation of CoP and ground reaction force/moment

Since the CoP is an important ground reference point for humanoid balance, equations to compute ground reaction force/moment and CoP are provided in numerous literatures (e.g., Abdallah & Goswami, 2005). However, for completeness we derive equations to compute CoP and ground reaction force/moment again using the notations used in this chapter.
The CoP is the point where the horizontal components of the moment generated by the ground reaction force (GRF) about the point vanish. The stationary humanoid robot can maintain balance when CoP is inside the supporting polygon given by the contact of feet and the ground. Since the GRF is unilateral, CoP is always in the support polygon. Assuming gravity $\boldsymbol{g}$ and GRF are the only external forces, GRF is $\boldsymbol{f_r} = M(\ddot{\boldsymbol{r}}_{\boldsymbol{G}} - \boldsymbol{g})$ where $\boldsymbol{r_G} = \frac{1}{M}\sum m_i \boldsymbol{T}_i \boldsymbol{c}_i$ is the CoM of a humanoid robot.
From the relations between the rate of change of angular momentum about the CoM $\dot{\boldsymbol{k}}_{\boldsymbol{G}}$ and the moment about the same point $\boldsymbol{m_G}$; i.e., $\dot{\boldsymbol{k}}_{\boldsymbol{G}} = \boldsymbol{m_G} = (\boldsymbol{r_P} - \boldsymbol{r_G}) \times \boldsymbol{f_r} + \boldsymbol{m_r}$ where $\boldsymbol{r_P}$ is CoP, and assuming the ground normal $\boldsymbol{n}$ is parallel to the gravity vector and locating spatial coordinate frame on the ground (i.e., $\boldsymbol{r_P} \perp \boldsymbol{n}$), we can compute the CoP and the vertical component of $\boldsymbol{m_r}$:

$$\boldsymbol{r_P} = \frac{1}{\boldsymbol{n} \cdot \boldsymbol{f_r}} \boldsymbol{n} \times \left(\dot{\boldsymbol{k}}_{\boldsymbol{G}} + \boldsymbol{r_G} \times \boldsymbol{f_r}\right)$$

$$\boldsymbol{n} \cdot \boldsymbol{m_r} = \boldsymbol{n} \cdot \left(\dot{\boldsymbol{k}}_{\boldsymbol{G}} + (\boldsymbol{r_G} - \boldsymbol{r_P}) \times \boldsymbol{f_r}\right).$$

9. References

Kajita, S.; Yamaura, T. & Kobayashi, A. (1992). Dynamic walk control of a biped robot along the potential energy conserving orbit, *IEEE Transactions on Robotics and Automation*, vol. 8, no. 4, pp. 431-438

Kajita, S.; Kanehiro, F.; Kaneko, K.; Fujiwara, K.; Yokoi, K. & Hirukawa, H. (2002). A realtime pattern generator for biped walking, *IEEE International Conference on Robotics and Automation (ICRA)*, pp. 31-37, Washington, DC, 2002

Sugihara, T. & Nakamura, Y. (2003). Variable impedant inverted pendulum model control for a seamless contact phase transition on humanoid robot, *IEEE International Conference on Humanoid Robots (Humanoids 2003)*, 2003

Komura, T.; Nagano, A.; Leung, H. & Shinagawa, Y. (2005a). Simulating pathological gait using the enhanced linear inverted pendulum model, *IEEE Transactions on Biomedical Engineering*, vol. 52, no. 9, pp. 1502-1513, September 2005

Abdallah, M. & Goswami, A. (2005). A biomechanically motivated two-phase strategy for biped robot upright balance control, *IEEE International Conference on Robotics and Automation (ICRA)*, pp. 3707-3713, Barcelona, Spain, April 2005

Kajita, S.; Kanehiro, F.; Kaneko, K.; Fujiwara, K.; Harada, K.; Yokoi, K. & Hirukawa, H. (2003). Resolved momentum control: Humanoid motion planning based on the linear and angular momentum, *IEEE/RSJ International Conference on Intelligent Robots and Systems*, pp. 1644—1650, Las Vegas, NV, USA, 2003

Vermeulen, J.; Verrelst, B.; Vanderborght, B.; Lefeber, D. & Guillaume, P. (2006). Trajectory planning for the walking biped "Lucy", *The International Journal of Robotics Research,* vol. 25, no. 9, pp. 867—887, 2006

Featherstone, R (1987). *Robot Dynamics Algorithms*, Kluwer Academic Publishers

Murray, R. M.; Li, Z. X. & Sastry S. S. (1994). *A Mathematical Introduction to Robotic Manipulation*, CRC Press

Ostrowski, J. (1999). Computing reduced equations for robotic systems with constraints and symmetries, *IEEE Transactions on Robotics and Automation*, vol. 15, no. 1, pp. 111--123, 1999

Crandall, S. H.; Karnopp, D.; Kurtz, E. F. & Pridmore-Brown, D. C. (1982). *Dynamics of Mechanical and Electromechanical Systems,* Krieger Publishing Company

Beer F. P. & Johnson, E. R. (1984). *Vector Mechanics for Engineers: Dynamics,* McGraw-Hill Book Company, New York

Cominoli, P. (2005). *Development of a physical simulation of a real humanoid robot,* Master's thesis, Swiss Federal Institute of Technology (EPFL), Lausanne

Sidi, M. J. (1997). *Spacecraft Dynamics and Control,* Cambridge University Press, New York

Astrom, K.; Block, A. & Spong, M. (2001). *The Reaction Wheel Pendulum*, Lecture Notes, Ed. Downloadable from: http://decision.csl.uiuc.edu/~spong/main.htm

Olfati-Saber, R. (2001). Stabilization of a flat underactuated system: the inertia wheel pendulum, *40th Conference on Decision and Control*, pp. 306--308, Orlando, FL, December 2001

Spong, M. W.; Corke, P. & Lozano, R. (2001). Nonlinear control of inertia wheel pendulum, *Automatica*, vol. 37, pp. 1845--1851, February 2001

Kuo, A. (1999). Stabilization of lateral motion in passive dynamic walking, *International Journal of Robotics Research*, vol. 18, no. 9, pp. 917--930, September 1999

Pratt, J. (2000). *Exploiting inherent robustness and natural dynamics in the control of bipedal walking robots*, Ph.D. dissertation, MIT

Komura, T.; Leung, H.; Kudoh, S. & Kuffner, J. (2005b). A feedback controller for biped humanoids that can counteract large perturbations during gait, *IEEE International Conference on Robotics and Automation (ICRA)*, pp. 2001--2007, Barcelona, Spain, 2005

Mayer, N. M.; Farkas, F. & Asada, M. (2005). Balanced walking and rapid movements in a biped robot by using a symmetric rotor and a brake, *International Conference on Mechatronics and Automation*, Niagara Falls, Ontario, Canada, July 2005

Walker, M. W. & Orin, D. (1982). Efficient dynamic computer simulation of robotic mechanisms, *ASME Journal of Dynamic Systems, Measurement, and Control*, vol. 104, pp. 205-211, September 1982

Lee, S.-H. & Goswami, A. (2007). Reaction Mass Pendulum (RMP): An explicit model for centroidal angular momentum of humanoid robots, *IEEE International Conference on Robotics and Automation (ICRA)*, pp. 4667-4672, Rome, Italy, 2007

Hofmann, A. (2005). *Robust Execution of Bipedal Walking Tasks from Biomechanical Principles*, Ph.D. dissertation, MIT